Journal of Computational Physics 242 (2013) 124–137

Contents lists available at SciVerse ScienceDirect

Journal of Computational Physics

journal homepage: www.elsevier.com/locate/jcp

A new fractional time-stepping method for variable density incompressible flows ☆

Ying Li [a], Liquan Mei [a,b,*], Jiatai Ge [a], Feng Shi [c]

[a] School of Mathematics and Statistics, Xi'an Jiaotong University, Xi'an 710049, China
[b] Center for Computational Geosciences, Xi'an Jiaotong University, Xi'an 710049,China
[c] Shenzhen Institutes of Advanced Technology, Chinese Academy of Sciences, Shenzhen 518055, China

ARTICLE INFO

Article history:
Received 22 June 2012
Received in revised form 3 February 2013
Accepted 11 February 2013
Available online 20 February 2013

Keywords:
Variable density incompressible flows
Naiver–Stokes equations
Finite element
Fractional time-stepping method

ABSTRACT

This paper describes a new method for solving variable density incompressible viscous flows. We have dealt with the momentum equation and the divergence free constraint in a new manner by rewriting the original equations. The originality of the proposed approach is that we have used different numerical methods to evaluate the evolution of the velocity and pressure. Compared with some established methods, the proposed approach is parameter-free, more flexible and can avoid the difficulties caused by the original equations. The stability analysis of the method is performed to show that our method is stable. Finally, numerical experiments are given to show the accuracy, efficiency and validness of this method for variable density incompressible flows.

1. Introduction

Variable density incompressible Navier–Stokes equations are widely used in the fields of fluid dynamics: for instance, in highly stratified flows, in the study of the dynamics of interfaces between fluids with different density, and in problems of inertial confinement and problems of astrophysics. However, very few papers have been dedicated to this problem. This paper deals with the numerical approximation of incompressible viscous flows with variable density. This type of flows are governed by the time-dependent Navier–Stokes equations [1,2]:

$$\begin{cases} \rho_t + \nabla \cdot (\rho \mathbf{u}) = 0, \\ \rho(\mathbf{u}_t + \mathbf{u} \cdot \nabla \mathbf{u}) + \nabla p - \nu \Delta \mathbf{u} = f, \\ \nabla \cdot \mathbf{u} = 0, \end{cases} \tag{1.1}$$

where the dependent variables are the density $\rho > 0$, the velocity field $\mathbf{u}$, and the pressure p. The constant ν is the dynamic viscosity coefficient and f is a driving external force. In stratified flows we typically have $f = \rho g$, where g is the gravity field. The fluid occupies a bounded domain Ω in $\mathbb{R}^d$ (with $d = 2$ or 3) and the solution of the above problem is sought on a time interval $[0, T]$. The Navier–Stokes system is supplemented by the following initial and boundary conditions for $\mathbf{u}$ and ρ:

$$\begin{cases} \rho(\mathbf{x}, 0) = \rho_0(\mathbf{x}), \quad \rho(\mathbf{x}, t)|_{\Gamma^-} = a(\mathbf{x}, t), \\ \mathbf{u}(\mathbf{x}, 0) = \mathbf{u}_0(\mathbf{x}), \quad \mathbf{u}(\mathbf{x}, t)|_{\Gamma} = \mathbf{b}(\mathbf{x}, t), \end{cases} \tag{1.2}$$

☆ The project is supported by NSF of China (10971164) and (11271234), The Fundamental Research Funds for the Central Universities (xjj20100112).
* Corresponding author at: School of Mathematics and Statistics, Xi'an Jiaotong University, Xi'an 710049, China. Tel.: +86 29 82669051.
E-mail address: lqmei@mail.xjtu.edu.cn (L. Mei).

0021-9991/$ - see front matter © 2013 Elsevier Inc. All rights reserved.
http://dx.doi.org/10.1016/j.jcp.2013.02.010

where $\Gamma = \partial\Omega$ and Γ^- is the inflow boundary, which is defined by $\Gamma^- = \{\mathbf{x} \in \Gamma;\ \mathbf{u}(\mathbf{x}) \cdot \mathbf{n} < 0\}$, with $\mathbf{n}$ being the outward unit normal vector. Throughout this paper we assume that the boundary Γ is impermeable, i.e., $\mathbf{u} \cdot \mathbf{n} = 0$ everywhere on Γ, and $\Gamma^- = \emptyset$. We note that no initial and boundary condition is needed for the pressure p, which can be viewed as a Lagrange multiplier whose mathematical role is to enforce the incompressibility condition.

The simulation of the system (1.1) and (1.2) presents the difficulty of satisfying the property of mass conservation twice. On one hand, the mass density of each fluid particle must remain unchanged during the fluid motion, whatever the level of unsteadiness and mixing. On the other hand, the velocity field must satisfy the incompressibility constraint, which reflects the unability of pressure to do compression work. These two important physical characteristics are fully described by the set of incompressible Navier–Stokes equations augmented by the advection equation for the density [3]. Therefore, how to construct stable and efficient numerical schemes for the system (1.1) and (1.2) is challenging.

For the mathematical theory of existence and uniqueness of solutions to this set of equations, we refer to Guermond [3] and Lions [4] for further details. This theory is very difficult, because the equations governing the motion of the incompressible fluid with variable density constitute a mixed PDE system entangling hyperbolic, parabolic, and elliptic features. Approximating (1.1) and (1.2) efficiently is a challenging task. A testimony of the difficulty is that, so far, very few papers have been dedicated to the mathematical analysis of the approximation of (1.1) and (1.2). We refer to Liu [5] and Guermond [6–8] for one of the few attempts in this direction.

For developing numerical approximations to this problem, it seems natural to exploit, as far as possible, the techniques established for the solution of constant density incompressible Navier–Stokes equations, viz., the fractional step projection method of Chorin [9,10] and Temam [11,12]. The method uses a time splitting, solving separately the transport equation for the density and the momentum for the velocity, the incompressible constraint being treated through a projection method, see [6]. This is the methodology followed in [3,13–15]. Several algorithms have been developed which extend this idea to the situation that concerns us here, see for example [1–3,16,17]. Caterina introduce an hybrid scheme which combines a finite volume approach for treating the mass conservation equation and a finite element method to deal with the momentum equation and the divergence free constraint [18]. To the best of our knowledge, Guermond and Quartapelle [3] gave the first stability proof of a projection method for variable density flows. The algorithm proposed in [3] is somewhat expensive since it is composed of two time-consuming projections. An alternative algorithm composed of only one projection per time step was proposed in [2] and had been proved to be stable.

These approaches have been used in some papers for incompressible flows with variable density. However, the variable density introduces considerable difficulties for the construction and analysis of accurate and stable projection type schemes. For example, it is well-known that the skew-symmetry of the nonlinear term in the Navier–Stokes equations (with constant density ρ_0), namely,

$$\int_\Omega (\rho_0 \mathbf{u} \cdot \nabla)\mathbf{v} \cdot \mathbf{v} dx = 0 \text{ for } \mathbf{u}, \mathbf{v} \text{ smooth enough and } \mathbf{u} \cdot \mathbf{n}|_\Gamma = 0$$

plays a very important role in the analysis of the Navier–Stokes equations and the corresponding numerical schemes. However, this property no longer holds when ρ is not a constant.

The objective of the present work is to introduce a new method for solving variable density flows. Many researchers have done a lot of work about Navier–Stokes system with constant density, for example [19–21]. We can try to use these methods to the variable density incompressible flows. In this paper, we proposed a new fractional time-stepping method for variable density incompressible flows.

The originality of our work is that we will use different numerical methods to evaluate the evolution of the velocity driven by the last two equations in the system (1.1). To be more specific, we solve the last two equations for a given density by the new fractional time-stepping method with time-splitting. The proposed algorithm is proved to be stable and numerically illustrated. The results show that this method is efficient.

The paper is organized as follows. In next section, we introduce some notations and preliminary results for this paper. In Section 3, a detailed presentation of the new method is given. In Section 4, the stability of the method is proved. In Section 5, a series of numerical experiments are given. The last section is devoted to concluding remarks.

2. Preliminary settings

2.1. Some notations

In this section, we aim to describe some of the notations which will be frequently used in this paper. We consider the time-dependent variable density Navier–Stokes system (1.1) and (1.2) on the finite time interval $[0, T]$ and in an open connected and bounded domain $\Omega \subset \mathbb{R}^d$ ($d = 2$ or 3) with boundary Γ, which we assume to be sufficiently smooth. More precisely, we assume that Ω is such that the Stokes operator possesses the usual regularization properties (see [22–24]).

For the mathematical setting of problem (1.1), we introduce the following Hilbert spaces:

$$H_0^1(\Omega) = \{v \in H^1(\Omega) : v|_{\partial\Omega} = 0\}$$

$$L_0^2(\Omega) = \{q \in L^2(\Omega) : \int_\Omega q dx = 0\}$$

For simplicity, set $W = H^1(\Omega),\ X = [H_0^1(\Omega)]^2,\ M = L_0^2(\Omega)$. Here, the spaces W and X are equipped with their usual scalar product and equivalent norm $(\nabla \mathbf{u}, \nabla \mathbf{v}),\ \|\mathbf{u}\|_{H_0^1} = \|\nabla \mathbf{u}\|_0$ for $\mathbf{u}, \mathbf{v} \in X$. Here, $\|\cdot\|_i$ and $|\cdot|_i$ denote the usual norm and semi norm of the Sobolev space $H^i(\Omega)$ or $H^i(\Omega)^d$, respectively, for $i = 0, 1, 2$. We define $A\mathbf{u} = -\Delta \mathbf{u}$. In particular, there holds

$$(A^{1/2}\mathbf{u}, A^{1/2}\mathbf{v}) = (\nabla \mathbf{u}, \nabla \mathbf{v}), \quad \forall \mathbf{u}, \mathbf{v} \in X$$

Moreover, we define the continuous bilinear forms $a(\cdot,\cdot)$ and $d(\cdot,\cdot)$ on $X \times X$ and $X \times M$, respectively, by

$$a(\mathbf{u}, \mathbf{v}) = v(\nabla \mathbf{u}, \nabla \mathbf{v}), \quad \mathbf{u}, \mathbf{v} \in X,$$
$$d(\mathbf{v}, q) = (q, \nabla \cdot \mathbf{v}), \quad \mathbf{v} \in X,\ q \in M$$

and a trilinear form on $X \times X \times X$ by

$$b(\mathbf{u}, \mathbf{v}, \mathbf{w}) = ((\mathbf{u} \cdot \nabla)\mathbf{v}, \mathbf{w}), \quad \mathbf{u}, \mathbf{v}, \mathbf{w} \in X.$$

$$\tilde{b}(\mathbf{u}, \mathbf{v}, \mathbf{w}) = (\mathbf{u}(\nabla \cdot \mathbf{v}), \mathbf{w}), \quad \mathbf{u}, \mathbf{v}, \mathbf{w} \in X.$$

Obviously, the bilinear $a(\cdot,\cdot)$ is continuous and coercive on $X \times X$ and the bilinear $d(\cdot,\cdot)$ is continuous on $X \times M$ and satisfies the well-known inf-sup condition [24,25]: there exists a positive constant $\beta_0 > 0$ such that for all $q \in M$

$$\sup_{\mathbf{v} \in X} \frac{|d(\mathbf{v}, q)|}{\|\nabla \mathbf{v}\|_0} \geqslant \beta_0 \|q\|_0, \tag{2.1}$$

where $d(\mathbf{v}, q) = (q, \nabla \cdot \mathbf{v})$. It is easy to verify that b satisfies the following important property [23]:

$$|b(\mathbf{u}, \mathbf{v}, \mathbf{w})| \leqslant c\|\nabla \mathbf{u}\|_0 \|\nabla \mathbf{v}\|_0 \|\nabla \mathbf{w}\|_0, \quad \forall \mathbf{u}, \mathbf{v}, \mathbf{w} \in X,$$

where $c > 0$ is a constant depending only on Ω. Henceforth c denotes a generic constant whose value may change at different occurrence.

2.2. The heuristics

To ensure the conservation of the density the L^2-norm and the balance of the kinetic energy for the variable density incompressible flows, Guermond and Quartapelle presented a equivalent system in the conserved form in their pioneering work [3]; See also Guermond and Salgado [1], Pyo and Shen [2] for the brief introduction. Our new time splitting scheme presented in the next section will also base on this conserved system. To make our presentation more clearly, we recall some introductions and observations of this conserved system.

First, we observe the mass conservation equation, namely the first equation of the system (1.1), and using the incompressibility of the velocity field, it can be rewritten in the non-conservative form:

$$\frac{\partial \rho}{\partial t} + \mathbf{u} \cdot \nabla \rho = 0, \tag{2.2}$$

one can deduce the boundedness of $\rho(r, t)$ if $\rho_0(r)$ is bounded, namely, if

$$0 < \alpha \leqslant \rho_0(r) \leqslant \beta, \quad \forall r \in \Omega, \tag{2.3}$$

then there holds that $0 < \alpha \leqslant \rho(r, t) \leqslant \beta$ for any $t > 0$.

When multiplying Eq. (2.2) by ρ and integrating the resulting equation over Ω, one can obtain

$$\int_\Omega \rho \frac{\partial \rho}{\partial t} + \int_\Omega \rho \mathbf{u} \cdot \nabla \rho = \frac{d}{dt}\left(\frac{1}{2}\int_\Omega \rho^2\right) = 0, \tag{2.4}$$

here the result

$$\int_\Omega \rho \mathbf{u} \cdot \nabla \rho = \frac{1}{2}\int_\Omega \mathbf{u} \cdot \nabla(\rho^2) = 0$$

is used by virtue of integration by parts, the incompressibility condition and the boundary condition for the normal component of velocity $\mathbf{n} \cdot \mathbf{u}|_\Omega = 0$. From (2.4), one can immediately deduce that

$$\|\rho(\cdot, t)\|_0 = \|\rho_0\|_0, \tag{2.5}$$

namely the conservation of the density in the L^2-norm, which needs to use the incompressibility condition. Hence, this property will be lost at the discrete level because the incompressibility constraint will be enforced weakly only. To bypass this trouble, one can rewrite the term $\mathbf{u} \cdot \nabla \rho$ in Eq. (2.2) in its skew-symmetric form $\mathbf{u} \cdot \nabla \rho + \rho \nabla \cdot \mathbf{u}/2$ by involving the incompressibility condition directly, i.e.,

$$\frac{\partial \rho}{\partial t} + \mathbf{u} \cdot \nabla \rho + \frac{\rho}{2} \nabla \cdot \mathbf{u} = 0. \tag{2.6}$$

As verified by Guermond and Quartapelle in [3], the mass conservation equation of this form can ensure the conservation of the density ρ in L^2 norm in time without invoking the incompressibility condition. Due to this property, the conservation of the density can be kept at the discrete level.

As to the momentum equation, following [3], to make the argument more clearly, the force $\mathbf{f}$ is assumed to be zero. Now multiplying the second equation of (1.1) by $\mathbf{u}$ and integrating over Ω, one can obtain

$$\int_\Omega \rho(\mathbf{u}_t + \mathbf{u} \cdot \nabla \mathbf{u}) \cdot \mathbf{u} + \int_\Omega \nabla p \cdot \mathbf{u} + \nu \int_\Omega |\nabla \mathbf{u}|^2 = 0. \tag{2.7}$$

By integration by parts and the conditions $\mathbf{u} \cdot \mathbf{n} = 0$ on $\Gamma = \partial\Omega$ and incompressibility $\nabla \cdot \mathbf{u} = 0$, the second term vanishes. This is still true at the discrete level due to the weak imposition of the incompressibility condition. Meanwhile, from integration by parts and (2.6), one can deduce

$$\int_\Omega \rho \mathbf{u}_t \cdot \mathbf{u} = \frac{1}{2} \int_\Omega \rho \frac{\partial |\mathbf{u}|^2}{\partial t} = \frac{1}{2} \int_\Omega \left(\frac{\partial (\rho |\mathbf{u}|^2)}{\partial t} + (\mathbf{u} \cdot \nabla \rho + \frac{\rho}{2} \nabla \cdot \mathbf{u}) |\mathbf{u}|^2 \right)$$

and

$$\int_\Omega \rho \mathbf{u} \cdot \nabla \mathbf{u} \cdot \mathbf{u} = \frac{1}{2} \int_\Omega \rho \mathbf{u} \cdot \nabla |\mathbf{u}|^2 = \frac{1}{2} \int_\Omega \left(\nabla \cdot (\rho \mathbf{u} |\mathbf{u}|^2) - (\mathbf{u} \cdot \nabla \rho + \rho \nabla \cdot \mathbf{u}) |\mathbf{u}|^2 \right).$$

Hence, under the condition $\mathbf{u} \cdot \mathbf{n} = 0$, the first term in (2.7) becomes

$$\int_\Omega \rho(\mathbf{u}_t + \mathbf{u} \cdot \nabla \mathbf{u}) \cdot \mathbf{u} = \frac{1}{2} \int_\Omega \nabla \cdot (\rho \mathbf{u} |\mathbf{u}|^2) - \frac{1}{4} \int_\Omega \rho \nabla \cdot \mathbf{u} |\mathbf{u}|^2. \tag{2.8}$$

To this end, when involving the incompressibility condition, (2.7) gives

$$\frac{1}{2} \int_\Omega \frac{\partial (\rho |\mathbf{u}|^2)}{\partial t} + \nu \int_\Omega |\nabla \mathbf{u}|^2 = 0,$$

which yields the control of the kinetic energy $\int_\Omega \rho |\mathbf{u}|^2 \leqslant \int_\Omega \rho_0 |\mathbf{u_0}|^2$ immediately. However, in view of (2.8), this property can also be guaranteed (especially at the discrete level) without the imposition of the incompressibility condition by modifying the original momentum equation with adding the nonlinear term $1/4 \int_\Omega \rho (\nabla \cdot \mathbf{u}) \mathbf{u}$. Noting that this tricky technique is unnecessary for constant density incompressible flows due to the skew-symmetric property of the trilinear term involving the nonlinear convective part $\rho \mathbf{u} \cdot \nabla \mathbf{u}$.

In conclusion, the complete equation system of the variable density incompressible flows for developing unconditionally stable integration schemes can be written as the following system in a conserved form

$$\begin{cases} \frac{\partial \rho}{\partial t} + \mathbf{u} \cdot \bigtriangledown \rho + \frac{\rho}{2} \nabla \cdot \mathbf{u} = 0, \\ \rho \left(\frac{\partial \mathbf{u}}{\partial t} + \mathbf{u} \cdot \bigtriangledown \mathbf{u} \right) + \nabla p - \nu \Delta \mathbf{u} + \frac{\rho}{4} (\nabla \cdot \mathbf{u}) \mathbf{u} = \mathbf{f}, \\ \nabla \cdot \mathbf{u} = 0. \end{cases} \tag{2.9}$$

In the above Eqs. (2.9), the additional terms $\frac{\rho}{2} \nabla \cdot \mathbf{u}$ and $\frac{\rho}{4} (\nabla \cdot \mathbf{u}) \mathbf{u}$ are consistent since they are all zero if $\nabla \cdot \mathbf{u} = 0$, and its meaning will become clear when doing the stability analysis as indicated by Guermond and Salgado [1, Proof of Theorem 2.1].

3. Description of our new numerical scheme

In this section, we shall propose a new fractional time-stepping method for variable density incompressible flows by referring the treatment technology of constant density flows and the technique used by Guermond and Salgado for variable density flows in reference [1]. The method uses a time splitting, solving separately the transport equation for the density in the first equation of (2.9) and the momentum in the second equation of (2.9). A first-order backward difference (BDF) for the temporal term is used. The velocity and pressure fields are computed simultaneously for the resolution of the last two equations in (2.9). We now describe the iterative methods that we proposed.

3.1. Our time splitting method

Let $\tau > 0$ be a time step and let us set $t_n = n\tau$ for $0 \leqslant n \leqslant N := [T/\tau]$. Let E be a normed space equipped with the norm $\|\cdot\|_E$. The space of functions $\phi : [0, T] \to E$ such that $t \in (0, T)$, the map $t \to \|\phi(t)\|_E \in R$ is L^p-integrable, is indifferently denoted $L^p((0, T); E)$ or $L^p(E)$. For any time-dependent function ϕ, we denote

$$\phi_h^k = \phi_h^k(t^k), \quad \phi^k := \phi(t^k), \quad k = 0, 1, 2, \ldots, N.$$

Now, we first present our time splitting method as follows. Set $\rho^0 = \rho_0,\ \mathbf{u}^0 = \mathbf{u}_0$, repeat the two following steps for $0 \leqslant n \leqslant N \leqslant T/\tau - 1$.

Step 1. Solve new density field:
Find $\rho^{n+1} \in W$ as the solution of

$$\begin{cases} \frac{\rho^{n+1}-\rho^n}{\tau} + \mathbf{u}^n \cdot \nabla \rho^{n+1} + \frac{\rho^{n+1}}{2} \nabla \cdot \mathbf{u}^n = 0, \\ \rho^{n+1}|_{\Gamma_-} = a(x, t^{n+1}). \end{cases} \tag{3.1}$$

Step 2. Solve new velocity and pressure fields:
Find $(\mathbf{u}^{n+1}, p^{n+1}) \in \mathbf{X} \times M$ as the solution of

$$\begin{cases} \rho^n \frac{\mathbf{u}^{n+1}-\mathbf{u}^n}{\tau} + \rho^{n+1}\mathbf{u}^n \cdot \nabla \mathbf{u}^{n+1} + \nabla p^{n+1} - \nu \Delta \mathbf{u}^{n+1} \\ \qquad + \frac{\rho^{n+1}}{4}(\nabla \cdot \mathbf{u}^n)\mathbf{u}^{n+1} = \mathbf{f}^{n+1}, \\ \nabla \cdot \mathbf{u}^{n+1} = 0, \\ \mathbf{u}^{n+1}|_{\Gamma} = \mathbf{b}(x, t^{n+1}). \end{cases} \tag{3.2}$$

Then the above Eqs. (3.1) and (3.2) can be rewritten into the variational formulations by multiplying these equations with appropriate test functions and applying integration by parts as follows.

Step 1. Solve new density field:
Find $\rho^{n+1} \in W$ with $\rho^{n+1}|_{\Gamma_-} = a(x, t^{n+1})$, such that

$$\left(\frac{\rho^{n+1}-\rho^n}{\tau}, w\right) + (\mathbf{u}^n \cdot \nabla \rho^{n+1}, w) + \left(\frac{\rho^{n+1}}{2} \nabla \cdot \mathbf{u}^n, w\right) = 0 \tag{3.3}$$

for any $w \in W$ with $w|_{\Gamma_-} = 0$.

Step 2. Solve new velocity and pressure fields:
Find $(\mathbf{u}^{n+1}, p^{n+1}) \in \mathbf{X} \times M$ with $\mathbf{u}^{n+1}|_{\Gamma} = \mathbf{b}(x, t^{n+1})$, such that

$$\begin{aligned} &(\rho^n \mathbf{u}^{n+1}, \mathbf{v}) + \tau b(\rho^{n+1}\mathbf{u}^n, \mathbf{u}^{n+1}, \mathbf{v}) - \tau d(\mathbf{v}, p^{n+1}) + \frac{1}{4}\tau \tilde{b}(\rho^{n+1}\mathbf{u}^{n+1}, \mathbf{u}^n, \mathbf{v}) + \tau d(\mathbf{u}^{n+1}, q) + \tau a(\mathbf{u}^{n+1}, \mathbf{v}) \\ &= \tau(\mathbf{f}^{n+1}, \mathbf{v}) + (\rho^n \mathbf{u}^n, \mathbf{v}) \end{aligned} \tag{3.4}$$

for any $(\mathbf{v}, q) \in \mathbf{X} \times M$ with $\mathbf{v}|_{\Gamma} = 0$.

3.2. Finite element approximation

To construct a Galerkin approximation of (3.3) and (3.4), we introduce three sequences of finite-dimensional spaces $W_h,\ X_h,\ M_h$, for $h > 0$, with $W_h \subset W, X_h \subset X$ and $M_h \subset M$. We use $W_h,\ X_h$, and M_h to approximate the density, the velocity, and the pressure, respectively. Assume that the pair of spaces (X_h, M_h) satisfies the discrete inf–sup condition (cf. [24,25]). So, we introduce the following finite-dimensional spaces

$$\begin{aligned} W_h &= \{w_h \in C^0(\overline{\Omega}_h) \cap W |\ w_{h|_K} \in P_2(K),\ \forall K \in \mathcal{T}_h\}, \\ \mathbf{X}_h &= \{v_h \in [C^0(\overline{\Omega}_h)]^2 \cap X |\ v_{h|_K} \in [P_2(K)]^2,\ \forall K \in \mathcal{T}_h\}, \\ M_h &= \{q_h \in C^0(\overline{\Omega}_h) \cap M |\ q_{h|_K} \in P_1(K),\ \forall K \in \mathcal{T}_h\}, \end{aligned}$$

where $P_i(K),\ i = 1, 2$ represents continuous piecewise (bi) linear subspace on set K. Simultaneously, initial values $u_h^0 = P_h u_0$ and ρ_h^0 are given with the L^2-orthogonal projection [23].

With the above statements, the standard finite element (FE) approximation formulation of the equations [26] is given as follows.

Step 1: Solve new density field:
Find $\rho_h^{n+1} \in W_h$ with $\rho_h^{n+1}|_{\Gamma_-} = a(x, t^{n+1})$, such that

$$(\rho_h^{n+1}, w_h) + \tau(\mathbf{u}_h^n \cdot \nabla \rho_h^{n+1}, w_h) + \frac{1}{2}\tau(\rho_h^{n+1} \nabla \cdot \mathbf{u}_h^n, w_h) - (\rho_h^n, w_h) = 0 \tag{3.5}$$

for any $w_h \in W_h$ with $w_h|_{\Gamma_-} = 0$.

Step 2: Solve new velocity and pressure fields:
Find $(\mathbf{u}_h^{n+1}, p_h^{n+1}) \in \mathbf{X}_h \times M_h$ with $\mathbf{u}_h^{n+1}|_{\Gamma} = \mathbf{b}(x, t^{n+1})$, such that

$$(\rho_h^n \mathbf{u}_h^{n+1}, \mathbf{v}_h) + \tau b(\rho_h^{n+1}\mathbf{u}_h^n, \mathbf{u}_h^{n+1}, \mathbf{v}_h) - \tau d(\mathbf{v}_h, p_h^{n+1}) + \tau d(\mathbf{u}_h^{n+1}, q_h) + \frac{1}{4}\tau \tilde{b}(\rho_h^{n+1}\mathbf{u}_h^{n+1}, \mathbf{u}_h^n, \mathbf{v}_h) + \tau a(\mathbf{u}_h^{n+1}, \mathbf{v}_h)$$
$$= \tau(\mathbf{f}^{n+1}, \mathbf{v}_h) + (\rho_h^n \mathbf{u}_h^n, \mathbf{v}_h) \tag{3.6}$$

for all $(\mathbf{v}_h, q_h) \in \mathbf{X}_h \times M_h$ with $\mathbf{v}_h|_\Gamma = 0$.

In the next section, we will prove that the above algorithm is stable.

4. Stability analysis of the method

Given the initial data $(\rho_0, \mathbf{u}_0)$, we construct the approximate data $(\rho_h^0, \mathbf{u}_h^0, p_h^0) \in W_h \times \mathbf{X}_h \times M_h$, such that

$$\|\rho_0 - \rho_h^0\|_{L^\infty} + \|\mathbf{u}_0 - \mathbf{u}_h^0\|_{\mathbf{L}^2} + h\|\mathbf{u}_0 - \mathbf{u}_h^0\|_{\mathbf{H}^1} + h\|p_0 - p_h^0\|_{L^2} \leqslant ch^{l+1}. \tag{4.1}$$

The initial pressure p_h^0 can be computed by the pair $(\rho_0, \mathbf{u}_0)$, see [6] for more details.

Henceforth we assume that $\min_{x\in\Omega} \rho_0(x) > 0$ and the approximate density field ρ_h^0 satisfies the following property

$$\alpha \leqslant \rho_h^0 \leqslant \beta, \tag{4.2}$$

where the parameters α and β are assumed to satisfy the following property

$$\alpha \leqslant \min_{x\in\Omega} \rho_0(x), \quad \sup_{x\in\Omega} \rho_0(x) \leqslant \beta. \tag{4.3}$$

The following Lemma is a classical result, see Guermond [3].

Lemma 1. *For ϕ and $\mathbf{v}$ regular and $\mathbf{v}$ such that $\mathbf{n}\cdot\mathbf{v}|_\Gamma = 0$, we have*

$$\int_\Omega [\phi \mathbf{v}\cdot\nabla\phi + \frac{1}{2}\phi^2 \nabla\cdot\mathbf{v}] = 0.$$

Next, we start with the stability proof of the system. To avoid irrelevant technicalities, we assume that there is no external driving force, i.e., $\mathbf{f} = \mathbf{0}$.

Proposition 1. *For any $\tau > 0$ and any sequence of velocities $\mathbf{u}_h^n$, $n = 0, \ldots, N$ in $\mathbf{L}^\infty(\Omega)$ with bounded divergence and satisfying $\mathbf{u}_h^n \cdot \mathbf{n}|_\Gamma = 0$, the solution to Eq. (3.5) satisfies:*

$$\|\rho_h^N\|_0^2 + \sum_{k=0}^{N-1} \|\rho_h^{k+1} - \rho_h^k\|_0^2 = \|\rho_h^0\|_0^2. \tag{4.4}$$

Proof. Taking $w_h = 2\rho_h^{n+1}$ in (3.5) and using the identity $2a\cdot(a-b) = a^2 - b^2 + (a-b)^2$, we obtain

$$\|\rho_h^{n+1}\|_0^2 - \|\rho_h^n\|_0^2 + \|\rho_h^{n+1} - \rho_h^n\|_0^2 + 2\tau \int_\Omega \rho_h^{n+1}\mathbf{u}_h^n \cdot \nabla\rho_h^{n+1} + \tau \int_\Omega (\rho_h^{n+1})^2 \nabla\cdot\mathbf{u}_h^n = 0. \tag{4.5}$$

Taking into account the boundary condition on $\mathbf{u}_h^n$ and integrating by parts, owing to Lemma 1, we infer

$$2\tau \int_\Omega \rho_h^{n+1}\mathbf{u}_h^n \cdot \nabla\rho_h^{n+1} + \tau \int_\Omega (\rho_h^{n+1})^2 \nabla\cdot\mathbf{u}_h^n = 0.$$

So, we have

$$\|\rho_h^{n+1}\|_0^2 - \|\rho_h^n\|_0^2 + \|\rho_h^{n+1} - \rho_h^n\|_0^2 = 0. \tag{4.6}$$

Adding up the above equality (4.6) from $n = 0$ to $n = N-1$, we obtain the desired result. □

Using the above result, we obtain the following theorem.

Theorem 1. *For any $\tau > 0$, the solution ρ_h^n, $n = 1, 2, \ldots$, of Eq. (3.5) satisfies the following stability estimate*

$$\|\rho_h^{n+1}\|_0 \leqslant \|\rho_0\|_0. \tag{4.7}$$

Theorem 2. *Setting $\sigma^k = \sqrt{\rho_h^k}$, for any $\tau > 0$, the solution $\mathbf{u}_h^n$, $n = 1, 2, \ldots$, of Eq. (3.6) with $\mathbf{f} = \mathbf{0}$ satisfies the following stability estimate*

$$\sum_{k=1}^N \|\sigma^k \mathbf{u}_h^k\|_0^2 + 2\nu\tau \sum_{k=1}^N \|\nabla\mathbf{u}_h^k\|_0^2 \leqslant \|\sigma_0\mathbf{u}_0\|_0^2, \tag{4.8}$$

$$\|p_h^{n+1}\|_0 \leqslant c\|\sigma_0\|_0\|\sigma_0\mathbf{u}_0\|_0 + c\|\sigma_0\mathbf{u}_0\|_0^2(\|\rho_0\|_0 + 1). \tag{4.9}$$

Proof. Taking $\mathbf{v}_h = 2\mathbf{u}_h^{n+1}$ and $q_h = 2p_h$ in (3.6) and using the identity $2a\cdot(a-b) = a^2 - b^2 + (a-b)^2$, we obtain

$$\|\sigma^n\mathbf{u}_h^{n+1}\|_0^2 - \|\sigma^n\mathbf{u}_h^n\|_0^2 + \|\sigma^n(\mathbf{u}_h^{n+1} - \mathbf{u}_h^n)\|_0^2 + 2\nu\tau\|\nabla\mathbf{u}_h^{n+1}\|_0^2 + \frac{\tau}{2}\int_\Omega \rho_h^{n+1}(\nabla\cdot\mathbf{u}_h^n)|\mathbf{u}_h^{n+1}|^2 + \tau\int_\Omega \rho_h^{n+1}\mathbf{u}_h^n\cdot\nabla|\mathbf{u}_h^{n+1}|^2 = 0. \tag{4.10}$$

Next, we take $w_h = |\mathbf{u}_h^{n+1}|^2$ in (3.5) and use integration by parts to get

$$\|\sigma^{n+1}\mathbf{u}_h^{n+1}\|_0^2 - \|\sigma^n\mathbf{u}_h^{n+1}\|_0^2 - \tau\int_\Omega \rho_h^{n+1}\mathbf{u}_h^n\cdot\nabla|\mathbf{u}_h^{n+1}|^2 - \frac{\tau}{2}\int_\Omega \rho_h^{n+1}(\nabla\cdot\mathbf{u}_h^n)|\mathbf{u}_h^{n+1}|^2 = 0. \tag{4.11}$$

Adding up (4.10) and (4.11) we obtain

$$\|\sigma^{n+1}\mathbf{u}_h^{n+1}\|_0^2 - \|\sigma^n\mathbf{u}_h^n\|_0^2 + \|\sigma^n(\mathbf{u}_h^{n+1} - \mathbf{u}_h^n)\|_0^2 + 2\nu\tau\|\nabla\mathbf{u}_h^{n+1}\|_0^2 = 0, \tag{4.12}$$

Adding up over $n = 0, 1, \ldots, N-1$ gives

$$\sum_{k=1}^{N}\|\sigma^k\mathbf{u}_h^k\|_0^2 + 2\nu\tau\sum_{k=1}^{N}\|\nabla\mathbf{u}_h^k\|_0^2 \leqslant \|\sigma_0\mathbf{u}_0\|_0^2, \tag{4.13}$$

$$\sum_{k=1}^{N}\|\sigma^n(\mathbf{u}_h^{n+1} - \mathbf{u}_h^n)\|_0^2 \leqslant \|\sigma_0\mathbf{u}_0\|_0^2. \tag{4.14}$$

Next, taking $q_h = 0$ in (3.6), we get

$$d(\mathbf{v}, p) = (\rho_h^n(\mathbf{u}_h^{n+1} - \mathbf{u}_h^n), \mathbf{v}_h) + \tau b_1(\rho_h^{n+1}, \mathbf{u}_h^n, \mathbf{u}_h^{n+1}, \mathbf{v}_h) - \frac{\tau}{4}b_2(\rho_h^{n+1}\mathbf{u}_h^{n+1}, \mathbf{u}_h^n, \mathbf{v}_h) + \tau a(\mathbf{u}_h^{n+1}, \mathbf{v}_h). \tag{4.15}$$

Hereafter, we will use the Poincare inequality

$$\|\mathbf{v}\|_0 \leqslant c\|\nabla\mathbf{v}\|_0, \quad \forall\mathbf{v}\in\mathbf{X} \tag{4.16}$$

and the Agmon's inequality:

$$\|\mathbf{v}\|_{L^\infty}^2 \leqslant c\|\mathbf{v}\|_0\|A\mathbf{v}\|_0, \quad \forall\mathbf{v}\in(H^2(\Omega))^2\cap\mathbf{X}. \tag{4.17}$$

Using (4.13), (4.14), (4.16) and (4.17), we have

$$|(\rho_h^n(\mathbf{u}_h^{n+1} - \mathbf{u}_h^n), \mathbf{v}_h)| \leqslant c\|\sigma_0\|_0\|\sigma_0\mathbf{u}_0\|_0\|\nabla\mathbf{v}_h\|_0, \tag{4.18}$$

$$|\tau b_1(\rho_h^{n+1}, \mathbf{u}_h^n, \mathbf{u}_h^{n+1}, \mathbf{v}_h)| \leqslant c\tau\|\rho_0\|_0\|\sigma_0\mathbf{u}_0\|_0^2\|\nabla\mathbf{v}_h\|_0, \tag{4.19}$$

$$|\frac{\tau}{4}b_2(\rho_h^{n+1}\mathbf{u}_h^{n+1}, \mathbf{u}_h^n, \mathbf{v}_h)| \leqslant c\tau\|\rho_0\|_0\|\sigma_0\mathbf{u}_0\|_0^2\|\nabla\mathbf{v}_h\|_0, \tag{4.20}$$

$$|\tau a(\mathbf{u}_h^{n+1}, \mathbf{v}_h)| \leqslant c\|\sigma_0\mathbf{u}_0\|_0^2\|\nabla\mathbf{v}_h\|_0. \tag{4.21}$$

Combining these estimates with (4.15) and using the discrete inf–sup condition yield

$$\begin{aligned}\beta^*\|p_h^{n+1}\|_0 &\leqslant \sup_{\mathbf{v}_h\in\mathbf{X}}\frac{(\nabla\cdot\mathbf{v}_h, p_h^{n+1})}{\|\nabla\mathbf{v}_h\|_0} \leqslant c\|\sigma_0\|_0\|\sigma_0\mathbf{u}_0\|_0 + c\tau\|\rho_0\|_0\|\sigma_0\mathbf{u}_0\|_0^2 + c\|\sigma_0\mathbf{u}_0\|_0^2\\ &\leqslant c\|\sigma_0\|_0\|\sigma_0\mathbf{u}_0\|_0 + c\|\sigma_0\mathbf{u}_0\|_0^2(\|\rho_0\|_0 + 1).\end{aligned} \tag{4.22}$$

So, we obtain the desired stability result. □

5. Numerical simulations

In this section, we present a series of numerical results to illustrate the accuracy, efficiency and capability of the method proposed in this paper through one smooth problem with exact solution and three benchmark problems with no exact solutions, namely the problems of viscous Rayleigh–Taylor instability, falling bubble and sloshing tank. In all simulations, the problem domain Ω will be partitioned into uniform triangular elements and the (P_2, P_2, P_1) approximation for the density, the velocity, and the pressure respectively will be used.

Table 1
Rates of convergence and error with different mesh size.

$\frac{1}{h}$	$\frac{\|\rho-\rho_h\|_0}{\|\rho\|_0}$	Order	$\frac{\|\mathbf{u}-\mathbf{u}_h\|_0}{\|\mathbf{u}\|_0}$	Order	$\frac{\|\mathbf{u}-\mathbf{u}_h\|_1}{\|\mathbf{u}\|_1}$	Order	$\frac{\|p-p_h\|_0}{\|p\|_0}$	Order
8	1.13402e−4	/	1.52515e−4	/	4.40883e−3	/	4.6349e−3	/
16	2.11487e−5	2.4228	2.58468e−5	2.5609	1.46537e−3	1.5891	1.12378e−3	2.0442
24	6.07385e−6	3.0769	7.31649e−6	3.1126	6.20704e−4	2.1186	4.80086e−4	2.0976
32	2.25269e−6	3.4478	2.81756e−6	3.3171	3.07712e−4	2.4391	2.61307e−4	2.1144

5.1. Rates of convergence study

In order to test the accuracy of the algorithm proposed in this paper, we consider a problem with a known analytical solution. Solving the variable density Navier–Stokes equations (1.1) and (1.2) in the unit square $\Omega = [0,1] \times [0,1]$ in R^2, having the exact solution

$$\rho(x,y,t) = 2 + x\cos(\sin(t)) + y\sin(\sin(t)),$$

$$\mathbf{u}(x,y,t) = \begin{pmatrix} -y\cos(t) \\ x\cos(t) \end{pmatrix},$$

$$p(x,y,t) = \sin(x)\sin(y)\sin(t),$$

so that the right-hand side to the momentum equation is

$$\mathbf{f} = \begin{pmatrix} \rho(x,y,t)(y\sin(t) - x\cos^2(t)) + \cos(x)\sin(y)\sin(t) \\ -\rho(x,y,t)(x\sin(t) + y\cos^2(t) + \sin(x)\cos(y)\sin(t)) \end{pmatrix}.$$

We use the (P_2, P_2, P_1) approximation for the density, the velocity, and the pressure, respectively. We perform the accuracy tests with respect to τ, h and Re. The mesh partition of Ω into triangular element.

First, we solve the above mentioned problem for $T = 0.5$. The time step is chosen small enough so that the error from the discretization of time can be negligible compared to the space error. We give our results for different mesh size $h = h_{max}$, where h_{max} is the length of the largest edge of the mesh. We consider $Re = 1000$. The results are given in Table 1. The accuracy and convergence rate of results are displayed by means of the h. From Table 1, we can see that we obtained a better convergence rates compared with the results presented in the literature [18].

Secondly, computation are made on a fixed mesh size for different Reynolds number $(Re = 1000, 3000, 5000, 8000, 10000)$. Taking $h = \frac{1}{8}$, $h = \frac{1}{16}$, $h = \frac{1}{24}$, $h = \frac{1}{32}$, the results is presented in Fig. 1. From Fig. 1, we can see that the stability still keeps well when the Reynolds number increases. These demonstrate that our method is very effective for high Reynolds number.

Next, computation are made on a fixed mesh size and a fixed Reynolds number with different time steps. The computation has been performed for $0 \leqslant t \leqslant 1$. The mesh size is chosen small enough so that the error from the discretization in space is negligible compared to the time stepping error. The convergence results with respect to τ are plotted in Table 2. From Table 2, we can see that the simulation results coincided with the theory.

5.2. Viscous Rayleigh–Taylor instability

In this Subsection we will illustrate the performance of the method on a realistic problem, namely the Rayleigh–Taylor instability. The problem has been considered in [1,3,13,18] starting from the results and comments in [27]. We compute the development of the Rayleigh–Taylor instability in the viscous regime as documented by Tryggvason in [27]. This problem consists of two layers of fluid initially at rest in the gravity field. It occupies the domain

$$\Omega = (-d/2, d/2) \times (-2d, 2d),$$

which splits into two region with varying density, the heavier fluid superposed to the light one. The interface is slightly smoothed since we set at time $t = 0$:

$$\rho_0(x,y) = \frac{\rho_m + \rho_M}{2} + \frac{\rho_M - \rho_m}{2}\tanh\left(\frac{y - \eta(x)}{0.01d}\right),$$

with $\rho_M > \rho_m > 0$, and $\eta(x) = -0.1d\cos(2\pi x/d)$ the initial position of the perturbed interface. The difficulty of the problem essentially depends on:

(1) the density ratio between the light and the heavy fluid, which is measured by the so-called Atwood number

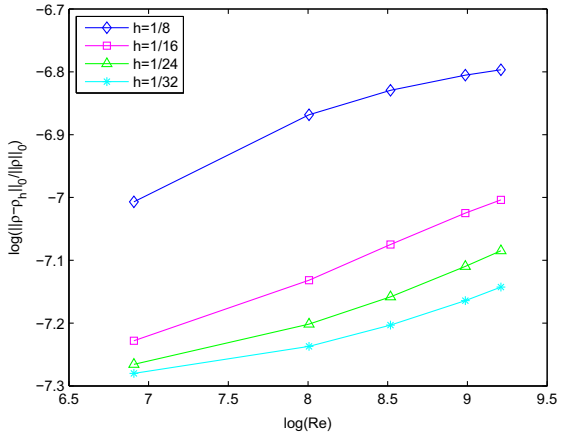

(a) L^2 error for the density

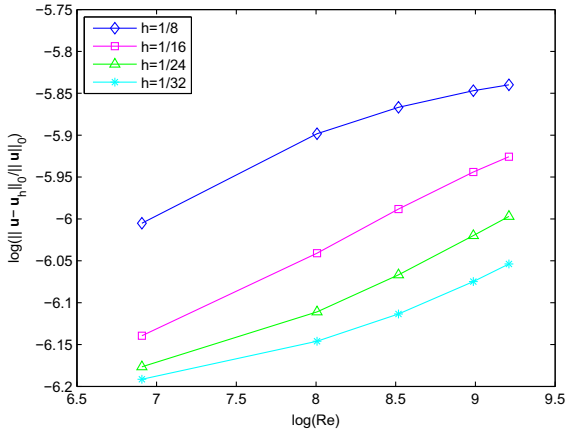

(b) L^2 error for the velocity

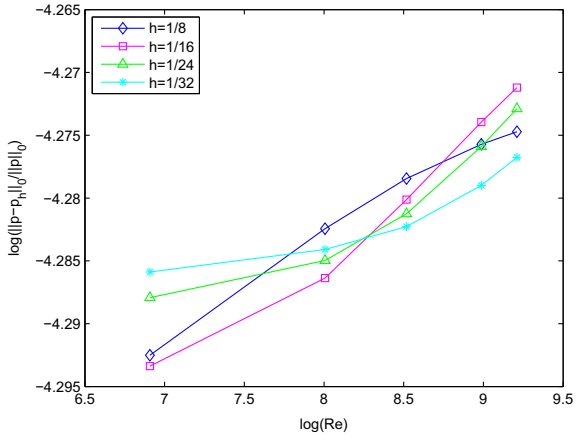

(c) L^2 error for the pressure

Fig. 1. Effect of varying h at different Reynolds number.

$$At = \frac{\rho_M - \rho_m}{\rho_M + \rho_m};$$

(2) the Reynolds number, defined as

Table 2
Rates of convergence and error in time.

τ	$\frac{\|\rho-\rho_h\|_0}{\|\rho\|_0}$	Order	$\frac{\|\mathbf{u}-\mathbf{u}_h\|_0}{\|\mathbf{u}\|_0}$	Order	$\frac{\|\mathbf{u}-\mathbf{u}_h\|_1}{\|\mathbf{u}\|_1}$	Order	$\frac{\|p-p_h\|_0}{\|p\|_0}$	Order
$\frac{1}{10}$	6.86335e−3	/	1.97172e−2	/	4.92798e−1	/	1.50103e−1	/
$\frac{1}{20}$	3.43669e−3	0.9979	1.00461e−2	0.9728	2.50629e−1	0.9754	7.15791e−2	1.0683
$\frac{1}{40}$	1.72141e−3	0.9974	5.07966e−3	0.9838	1.26527e−1	0.9861	3.49476e−2	1.0343
$\frac{1}{80}$	8.61434e−4	0.9988	2.55548e−3	0.9911	6.35873e−2	0.9926	1.72524e−2	1.0184
$\frac{1}{160}$	4.30589e−4	1.0004	1.2818e−3	0.9954	3.18886e−2	0.9957	8.55538e−3	1.0119
$\frac{1}{320}$	2.14937e−4	1.0024	6.41874e−4	0.9978	1.59896e−2	0.9959	4.24646e−3	1.0106

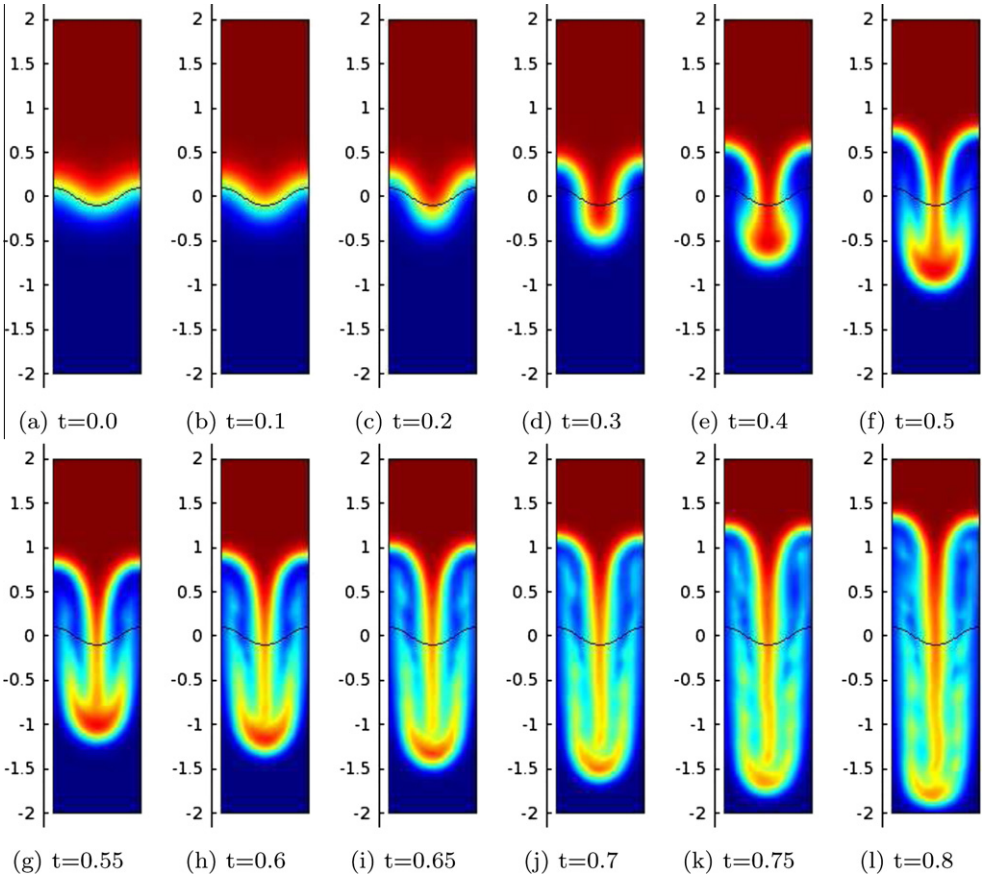

Fig. 2. The density field, $At = 0.5$ $(\rho_M = 3, \rho_m = 1)$, $Re = 1000$.

$$Re = \frac{\rho_m d^{3/2} g^{1/2}}{\mu};$$

where $\mu > 0$ is the dynamic viscosity of the fluid (supposed to be constant in the whole domain) and g is the gravitational acceleration. For $t > 0$ the system evolves under the action of a vertical downward gravity field of intensity g; the source term in the momentum equation is downward and equal to ρg.

The equations are made dimensionless by using the following references: ρ_m for the density, d for lengths, and $d^{1/2}/g^{1/2}$ for time. So, the reference velocity is $d^{1/2}g^{1/2}$. We assume that the symmetry of the initial condition is maintained during the time evolution. The no-slip condition is enforced at the bottom and top walls and symmetry is imposed on the two vertical sides.

Next, we compare the solutions obtained at different Atwood numbers.

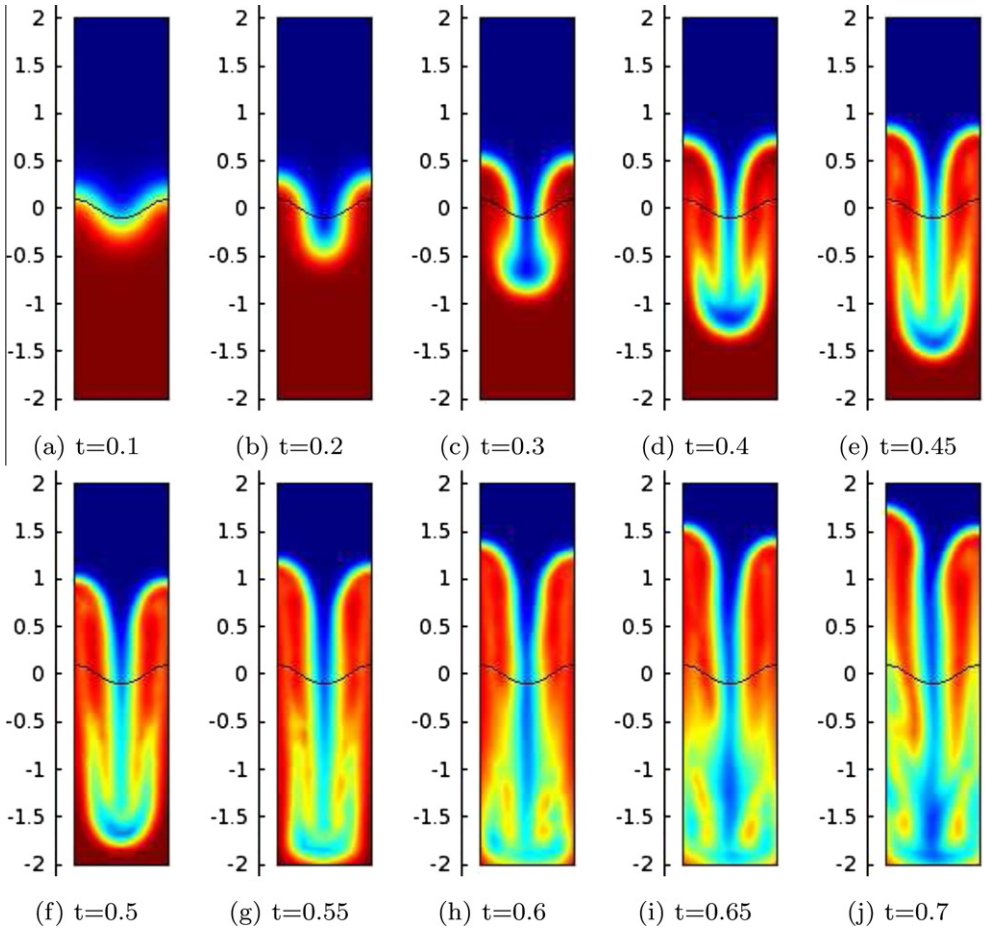

Fig. 3. The density field, $At = 0.75$ $(\rho_M = 7, \rho_m = 1)$, $Re = 1000$.

- *A low Atwood number problem*: Setting $At = 0.5$ $(\rho_M = 3, \rho_m = 1)$, $Re = 1000$. The time evolution of the interface of the density field is displayed in Fig. 2 at times 0.1, 0.2, 0.3, 0.4, 0.5, 0.55, 0.6, 0.65, 0.7, 0.75, 0.8. The results are very close to those in [1,3,7]. Compared to the old methods, the results show good agreement in the global characteristics of the flows. And we can only observe some slight difference at large times of the calculation.
- *A high Atwood number problem*: Setting $At = 0.75$ $(\rho_M = 7, \rho_m = 1)$, $Re = 1000$. For this situation, The time evolution of the interface of the density field is plotted in Fig. 3 at times 0.1, 0.2, 0.3, 0.4, 0.45, 0.5, 0.55, 0.6, 0.65, 0.7. Compared with the above test, we can observe the similar structure and the global characteristics of the flow in the early stage. At the same time, we found that the heavy fluid falls faster compared with the low Atwood number problem. The simulation results coincided with the law of physics and are very close to the results presented in the literature [1,3,7,18].
- *A very high Atwood number problem*: Setting $At = 0.9$ $(\rho_M = 19, \rho_m = 1)$, $Re = 1000$. As the Atwood value increases, the sensitiveness of the calculation to the numerical instabilities grows. The downward motion of the heavy fluid increases with the density difference. The time evolution of the interface of the density field is plotted in Fig. 4. It seems that the evolution of the interface configuration does not change significantly. But notice that at $At = 0.9$ it is very difficult to continue the simulation in the literature[18]. A series of numerical experiments are given to show that this method is more efficient.

5.3. Falling bubble test

To investigate the capability of our method to work with larger density variations, we give the computational results for falling bubble test. This simulation is inspired from [18,28]. A heavy "droplet" falls through a light fluid and impacts into the plane surface of the heavy fluid in a cavity. The computational domain is $(0, d) \times (0, 2d)$, where $d = 1$ and at $t = 0$ the fluid is at rest with density:

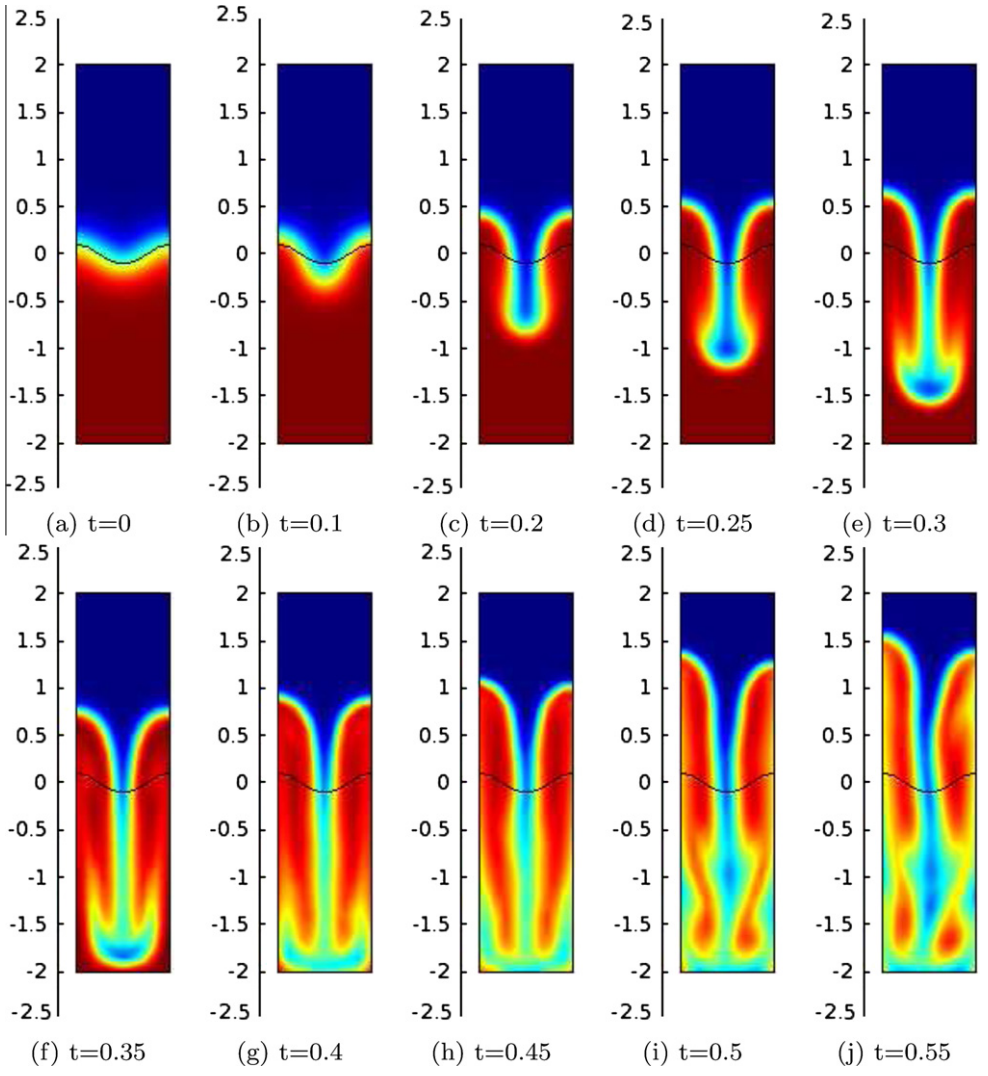

Fig. 4. The density field, $At = 0.9$ $(\rho_M = 19, \rho_m = 1)$, $Re = 1000$.

$$\rho(x,y) = \begin{cases} 100 & \text{if } 0 \leqslant y \leqslant 1 \quad \text{or} \quad 0 \leqslant r \leqslant 0.2, \\ 1 & \text{if } 1 < y \leqslant 2 \quad \text{and} \quad r \geqslant 0.2, \end{cases}$$

where $r = \sqrt{(x-0.5)^2 + (y-1.75)^2}$. As in [18,28], the equations are made dimensionless by using the following references: ρ_m for density, d for length, $\sqrt{d/g}$ for time, then, the reference velocity is $\sqrt{dg}$. In the dimensionless equations, the gravity term is $\mathbf{f} = (0, -\rho)^T$ and the Reynolds number is defined as in above Section. In our test, the viscosity of the fluid is supposed to be constant in the whole domain and we have $Re = 1000$.

The results are displayed in Fig. 5. The figure contain snapshots of the fluid interface. The snapshots show how the "droplet" travels up through a light fluid and merges with a light fluid below. As the "droplet" falls, its shape remains spherical due to the surface tension and the viscosity. As the droplet hits the interface, it merges with the light fluid below and creates waves on the surface. The simulation results show good agreement with the results presented in the literature.

5.4. Sloshing tank

To investigate the capability of our method to work with very large density variations, a two-fluid flow in a two-dimensional sloshing tank is considered in this Subsection. This test case was also investigated in [29,30]. Following [29,30], the problem domain is $\Omega = [-L, L] \times [-H, H]$, where $L = 0.5$ m and $H = 0.75$ m. The interface separating the two phase is initially given as

$$y = 0.26 + 0.1 \sin(\pi x).$$

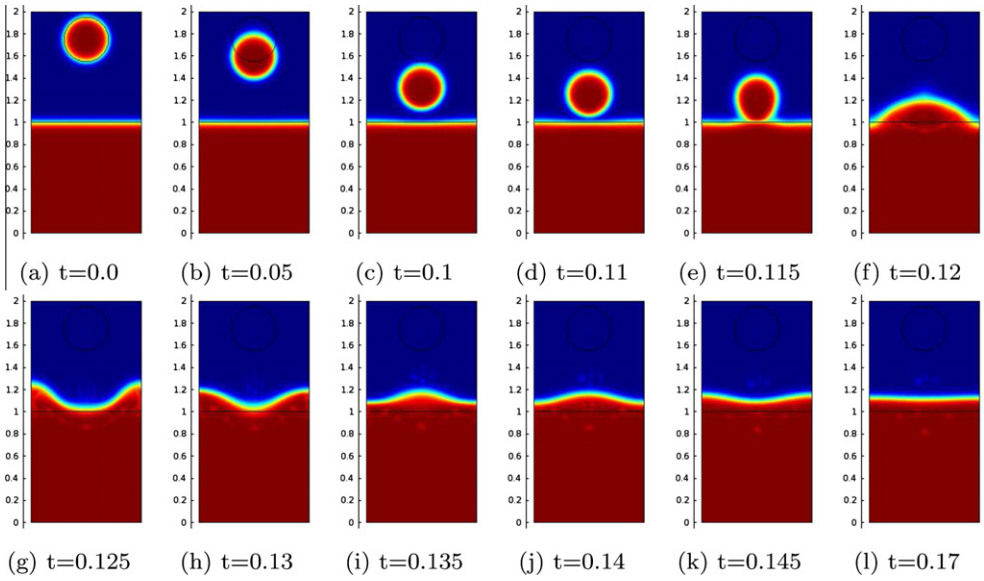

Fig. 5. The density field, $Re = 1000$.

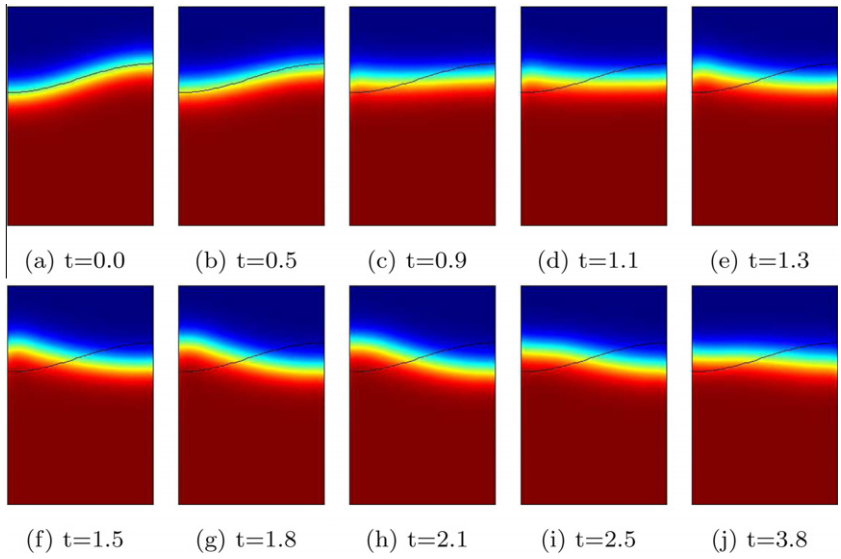

Fig. 6. The density field at different times.

The densities of the fluids are $\rho_1 = 1.0\ \mathrm{kg/m^3}$ and $\rho_2 = 1000.0\ \mathrm{kg/m^3}$, and the dynamic viscosities are $\mu_1 = 0.001\ \mathrm{kg/(ms)}$ and $\mu_2 = 1.0\ \mathrm{kg/(ms)}$. The lighter fluid superposed to the heavy one. No surface tension is considered here, so the volume force is $\mathbf{f} = (0, -0.1\ \mathrm{m/s^2})^T$. Slip-boundary conditions are assumed along the walls of the tank, and a zero velocity field is initially assumed. The spatial approximation is performed with $(P2, P2, P1)$ for density, velocity and pressure, respectively. The time-step length is $\tau = 0.015$ s and the situation is observed for $t = (0\ \mathrm{s}, 20\ \mathrm{s})$.

The results are displayed in Fig. 6. The evolution of the interface at selected points in time. For confirmation, these patterns may be compared to the respective patterns displayed Fig. 9 in [29] and Fig. 15 in [30], we can observe the similar results.

6. Conclusion

In this paper, we proposed a new fractional time-stepping method to the case of incompressible viscous flows with variable density. We have rewritten the momentum equation in a new form to guarantee that the spatial discretization errors

associated with the satisfaction of the mass conservation cannot affect the balance of the kinetic energy of the fluid. The originality of our approach is that we have used different numerical methods to evaluate the evolution of the velocity and pressure. The new method uses a time splitting scheme to separately solve the transport equation and the momentum equation. The new scheme has been used to solve the momentum equation associated to the divergence constraint by a finite element method. The stability proof of the method we proposed for variable density flows was given in the paper.

To verify the correctness of the method, we have applied it to the test cases previously considered in the literature. The spatial approximation is performed by means of Lagrangian finite elements with $P2$ interpolation for density and velocity and $P1$ interpolation for pressure. First, the rates of convergence of the method were given and we obtained a better convergence rates compared with the results presented. Then, the simulation of the viscous Rayleigh–Taylor instability was also investigated. The simulation results coincided with the law of physics and are very close to the results presented in the literature. Compared with some established methods, numerical results show that new method exhibited good stability behavior even for large time steps or the high Atwood number.

References

[1] J.L. Guermond, A. Salgado, A splitting method for incompressible flows with variable density based on a pressure Poisson equation, Journal of Computational Physics 228 (2009) 2834–2846.
[2] J.H. Pyo, J. Shen, Gauge–Uzawa methods for incompressible flows with variable density, Journal of Computational Physics 221 (2007) 181–197.
[3] J.L. Guermond, L. Quartapelle, A projection FEM for variable density incompressible flows, Journal of Computational Physics 165 (2000) 167–188.
[4] P.L. Lions, Mathematical Topics in Fluid Mechanics, Clarendon, Oxford, 1996.
[5] C. Liu, N.J. Walkington, Convergence of numerical approximations of the incompressible Navier–Stokes equations with variable density and viscosity, SIAM Journal on Numerical Analysis 45 (2007) 1287–1304.
[6] J.L. Guermond, P. Minev, J. Shen, An overview of projection methods for incompressible flows, Computer Methods in Applied Mechanics and Engineering 195 (2006) 6011–6045.
[7] J.L. Guermond, A. Salgado, A fractional step method based on a pressure Poisson equation for incompressible flows with variable density, Numerical Analysis (2008) 913–918.
[8] J.L. Guermond, A. Salgado, Error analysis of a fractional time-stepping technique for incompressible flows with variable density, SIAM Journal on Numerical Analysis 49 (2011) 917–940.
[9] A.J. Chorin, Numerical solution of the Navier–Stokes equations, Mathematics of Computation 22 (1968) 745–762.
[10] A.J. Chorin, On the convergence of discrete approximations to the Navier–Stokes equations, Mathematics of Computation 23 (1969) 341–353.
[11] R. Temam, Navier–Stokes Equations, Studies in Mathematics and Its Applications, vol. 2, North-Holland, Amsterdam, 1977.
[12] R. Temam, Sur l'approximation des quatious de Navier–Stokes par la mthode des pas fractionnaires (II)[J], Archive for Rational Mechanics and Analysis 33 (1969) 377–385.
[13] Y. Fraigneau, J.L. Guermond, L. Quartapelle, Approximation of variable density incompressible flows by means of finite elements and finite volumes, Communications in Numerical Methods in Engineering 17 (2001) 893–902.
[14] G.P. Puckett, A.S. Almgren, J.B. Bell, D.L. Marcus, W. Rider, A high-order projection method for tracking fluid interfaces in variable density incompressible flows, Journal of Computational Physics 130 (1997) 269–282.
[15] G.C. Buscaglia, R. Codina, Fourier analysis of an equal-order incompressible flow solver stabilized by pressure gradient projection, International Journal for Numerical Methods in Fluids 34 (2000) 65–92.
[16] J.B. Bell, D.L. Marcus, A second order projection method for variable-density flows, Journal of Computational Physics 101 (1992) 334–348.
[17] A.S. Almgren, J.B. Bell, P. Colella, L.H. Howell, M.L. Welcome, A conservative adaptive projection method for the variable density incompressible Navier–Stokes equations, Journal of Computational Physics 142 (1998) 1–46.
[18] C. Calgaro, E. Creuse, T. Goudon, An hybrid finite volume-finite element method for variable density incompressible flows, Journal of Computational Physics 227 (2008) 4671–4696.
[19] Y. He, J. Li, Convergence of three iterative methods based on the finite element discretization for the stationary Navier–Stokes equations, Computer Methods in Applied Mechanics and Engineering 198 (2009) 1351–1359.
[20] R. Codina, J. Blasco, G. Buscaglia, A. Huerta, Implementation of a stabilized finite element formulation for the incompressible Navier–Stokes equations based on a pressure gradient projection, International Journal for Numerical Methods in Fluids 37 (2001) 419–444.
[21] C. Dohrmann, P. Bochev, A stabilized finite element method for the Stokes problem based on polynomial pressure projections, International Journal for Numerical Methods in Fluids 46 (2004) 183–201.
[22] L. Cattabriga, Su un problema al contorno relativo al sistema di equazioni di Stokes, Rendiconti del Seminario Matematico della Universit di Padova 31 (1961) 308–340.
[23] R. Temam, Navier–Stokes Equations: Theory and Numerical Analysis, North-Holland, Amsterdam, 1984.
[24] V. Girault, P.A. Raviart, Finite Element Method for Navier–Stokes Equations: Theory and Algorithms, Springer-Verlag, Berlin, Heidelberg, 1986.
[25] A. Ern, J.L. Guermond, Theory and Practice of Finite Elements, Springer-Verlag, New York, 2004.
[26] Z. Chen, Finite Element Methods and Their Applications, Scientific Computation, Springer, Berlin, 2005.
[27] G. Tryggvason, Numerical simulations of the Rayleigh–Taylor instability, Journal of Computational Physics 75 (1988) 235–282.
[28] T. Schneider, N. Botta, K.J. Geratz, R. Klein, Extension of finite volume compressible flow solvers to multidimensional, variable density zero Mach number flows, Journal of Computational Physics 155 (1999) 248–286.
[29] U. Rasthofer, F. Henke, W.A. Wall, V. Gravemeier, An extended residual-based variational multiscale method for two-phase flow including surface tension, Computer Methods in Applied Mechanics and Engineering 200 (2011) 1866–1876.
[30] T.P. Fries, The intrinsic XFEM for two-phase flows, International Journal for Numerical Methods in Fluids 60 (2009) 437–471.